JOURNAL OF MATERIALS SCIENCE 22 (1987) 1437–1442

# The yield behaviour of amorphous polyethylene terephthalate: an activated rate theory approach

J. S. FOOT*, R. W. TRUSS‡, I. M. WARD, R. A. DUCKETT
*Department of Physics, University of Leeds, Leeds LS2 9JT, UK*

Yield-stress measurements on amorphous polyethylene terephthalate film are presented covering five decades of strain rate at temperatures from just below the glass transition (~60° C) to −160° C. The data were obtained by combining measurements from a conventional Instron machine with data from a high-speed tensile tester capable of applying strain rates of up to 50 $sec^{-1}$. Five different failure modes have been identified over this extensive range of test conditions. All data from tests which show a clear yield point can be described accurately by an extension of the Ree Eyring approach to include two processes. The process which is only important at low temperatures correlates well with the $\beta$-process observed in dynamic mechanical experiments.

## 1. Introduction

Many workers [1–5] have chosen to consider yielding in polymers as a thermally activated process, following the formalism developed by Eyring and coworkers [6] for creep at constant applied stress. On this dynamical view of the yield process, the yield stress denotes the point at which the internal viscosity falls to the value where the plastic strain rate equals the applied strain rate, $\dot{\varepsilon}$. We can then write

$$\dot{\varepsilon} = \dot{\varepsilon}_0 \exp(-\Delta H/kT) \sinh(\sigma_y v/kT) \quad (1)$$

where $\Delta H$ is the activation energy, $\sigma_y$ the yield stress (usually tensile or compressive), $v$ the activation volume, and $\dot{\varepsilon}_0$ is a constant pre-exponential factor. This gives the yield stress as

$$\sigma_y = (kT/v) \sinh^{-1}[(\dot{\varepsilon}/\dot{\varepsilon}_0) \exp(\Delta H/kT)] \quad (2)$$

which for high values of stress reduces to

$$\sigma_y = \Delta H/v + (kT/v) \ln(2\dot{\varepsilon}/\dot{\varepsilon}_0) \quad (3)$$

Extensive studies by Roetling [3] and by Bauwens-Crowet *et al.* [4] have shown that the yield stresses in general increase more rapidly at high strain rates and low temperatures than indicated by Equation 3. It has therefore been proposed that there is normally more than one activated rate process present with all species of flow units moving at the same rate, the stresses being additive. Equations 2 and 3 can then be combined for two activated processes to give

$$\sigma_y = (kT/v_1)[\Delta H_1/kT + \ln(2\dot{\varepsilon}/\dot{\varepsilon}_{01})] + (kT/v_2 \sinh^{-1}[(\dot{\varepsilon}/\dot{\varepsilon}_{02}) \exp(\Delta H_2/kT)] \quad (4)$$

where process 1 is considered to be in the high stress condition so that the sinh term can be simplified to an exponential.

In a previous paper [7], we analysed the yield behaviour of several grades of polyethylene in tension and torsion under pressure in terms of multiple Eyring processes operating in parallel. A more general form of Equation 4 was adopted where

$$\sigma_y/T = \sum_{i=1}^{N} (k/v_i) \sinh^{-1}[(\dot{\varepsilon}/\dot{\varepsilon}_{02}) \times \exp((\Delta H_i + p\Omega_i)/kT)] \quad (5)$$

where $v_i$ and $\Omega_i$ are the stress and pressure activation volumes, $\Delta H_i$ the activation energy and $\dot{\varepsilon}_{0i}$ is the pre-exponential factor for each process. For polyethylene $N = 3$, and processes were identified which could be associated with the $\alpha$ and $\gamma$ mechanical relaxations. Both the positions of the transitions in temperature/pressure/strain-rate space and the magnitudes of the activation energies of the Eyring processes were in good agreement with corresponding mechanical relaxations.

The success of this approach for polyethylene has led us to re-analyse data available in this laboratory for the yield behaviour of amorphous polyethylene terephthalate [8].

## 2. Experimental procedure

### 2.1. Preparation of tensile specimens

The dumb-bell tensile specimens were cut from polyethylene terephthalate (PET) sheet of thickness 0.020 to 0.025 cm to a gauge length of 2.54 cm and a gauge width of 0.4 cm. The PET sheet was amorphous and isotropic, the yield stress in the plane of the sheet being isotropic within experimental error. The sheet was supplied by Imperical Chemical Industries Ltd, Plastics Division, made from a polymer with an intrinsic viscosity of 0.60.

* *Present address*: Royal Aircraft Establishment, Materials Department, Farnborough, Hampshire GU14 6TD, UK.
‡ *Present address*: I.C.I. Australia, Melbourne, Australia.

0022–2461/87 $03.00 + .12 

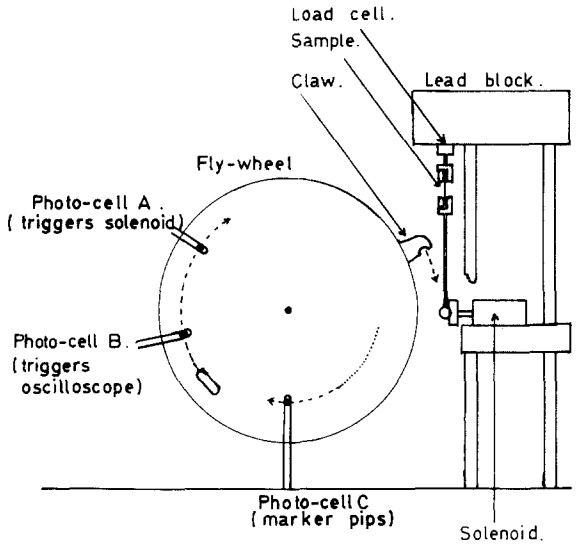


*Figure 1* Schematic diagram of the high-speed tensile tester (see text for explanation).

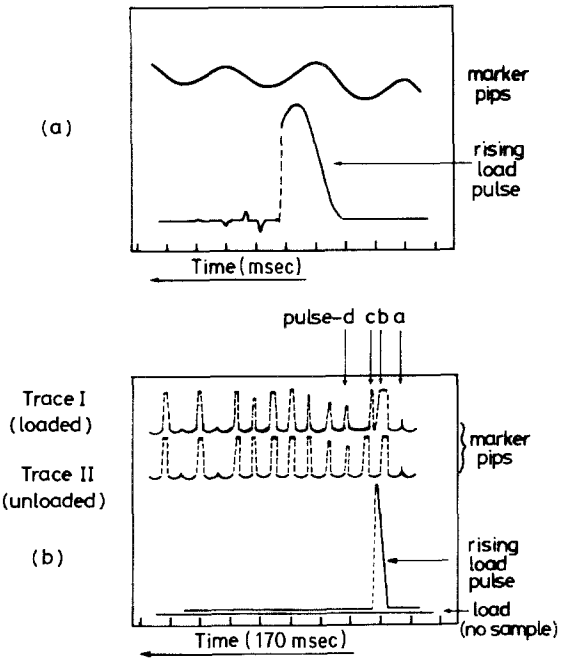


*Figure 2* Typical oscilloscope traces for (a) $\dot{\varepsilon} = 51\,\text{sec}^{-1}$, $T = 5°\,\text{C}$ and (b) $\dot{\varepsilon} = 0.8\,\text{sec}^{-1}$, $T = 22°\,\text{C}$. Time increases from right to left. See text for explanation.

## 2.2. Low strain-rate tests

The low strain-rate tests were performed on an Instron tensile testing machine over a range of displacement speeds from $2 \times 10^{-5}\,\text{cm sec}^{-1}$ to approximately $1\,\text{cm sec}^{-1}$. The load was displayed on a chart recorder as a function of time except for speeds above $0.2\,\text{cm sec}^{-1}$ where an oscilloscope and camera were used.

## 2.3. High strain-rate tests

For the high strain-rate tests, we have used a high-speed testing machine originally designed and built at British Cellophane Ltd, Bridgwater by Dr D. H. Morton and Mr J. M. Cass. The design was based on a similar machine built at Du Pont Ltd, which is described by Amorski and Mecca [9].

The principle is to accelerate a fly-wheel slowly to a desired speed and then to release the polymer sample into the path of a claw on its periphery. To ensure a constant strain rate, the energy of the system must greatly exceed that required to break the sample, which for the PET sheet samples reached 0.2 J. The main fly-wheel is driven through reduction gears of 1:1, 10:1 or 100:1 by an energy-bank fly-wheel powered by a 0.5 horse power (hp) variable speed motor, and claw speeds were achieved from 0.5 to $3000\,\text{cm sec}^{-1}$. Above $300\,\text{cm sec}^{-1}$ at least 20 J is stored in the energy-bank fly-wheel. Although heavy duty gears are used there is some slack between the two fly-whels ($\sim 0.2\,\text{cm}$ claw movement). At lower speeds there is sufficient time for the variable-speed motor to control the speed.

The arrangement is shown schematically in Fig. 1. Three photocells A, B and C are arranged on the periphery of the main fly-wheel. When the desired speed is reached, photocell A is used to trigger the solenoid holding the lower clamp from the claw. Photocell B triggers an oscilloscope just before the claw reaches this clamp, and photocell C measures the speed of the wheel by receiving light from a series of equally spaced holes drilled in the fly-wheel.

Fig. 2a shows a typical oscilloscope record of a tensile test. The upper trace is the load signal, showing a small amount of ripple from the load cell. The lower trace shows the marker pips from photocell C, which are smoothed out at this high speed. It is to be noted that at this speed there is no observed slowing down of the fly-wheel during the test.

Fig. 2b shows failure at a slower speed, where the effect of the slack between the main fly-wheel and the energy-bank fly-wheel is significant. Because the oscilloscope is always triggered at the same position of the fly-wheel, it was possible to record a second set of pips immediately after the tensile test. In Fig. 2b there are two traces at the bottom of the photograph, one with the rising load pulse, the second without it and almost superimposed on it. The top trace 1 is the set of marker pips when the sample is tested, the centre trace 2 is the same set of pips without the sample. Pulse a occurs at the same time after the triggering of the oscilloscope on both traces 1 and 2. Pulse b is extended on trace 1 compared to trace 2 due to the slack being taken up between the two fly wheels. Pulse c on trace 1 is shorter and occurs before the pulse on trace 2, because when the sample breaks the fly wheel moves to the other extreme of the slack. For pulse d and those after, traces 1 and 2 are coincident in time after triggering.

It is clear from these results that at the lowest strain rates there is some divergence from constant strain-rate conditions of test. However, the coincidence of traces 1 and 2 beyond pulse d shows that there is no slowing down of the energy-bank fly-wheel, and the rapid acceleration of the main fly-wheel after the sample break shows that the inertia of the main fly-wheel is small. We have therefore assumed that the strain-rate at the yield point, where the load is stationary, is determined by the speed of the energy-bank fly-wheel, i.e. using the trace from the unloaded fly-wheel. It is estimated that, taking into account these

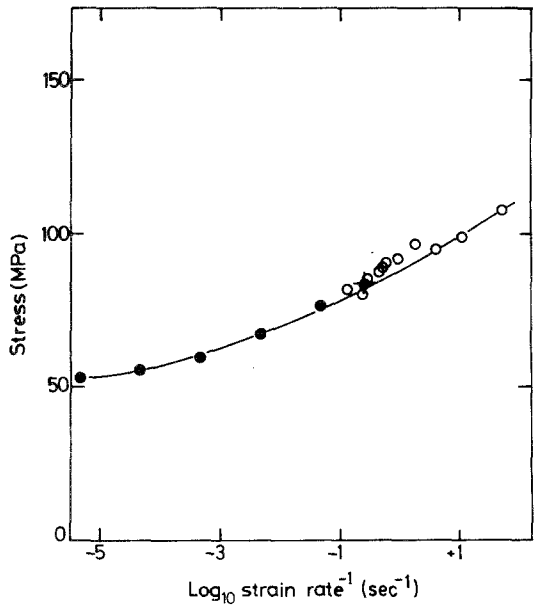


*Figure 3* Yield-stress data for PET at $T = 22 \pm 2°$ C. The experimental results were obtained using a conventional Instron at low strain-rates (●) and using the high-speed tensile tester at high strain-rates (○). The result marked (+) was obtained on the Instron making use of an oscilloscope recorder.

errors in strain rate at low strain rates, the determination of strain and strain rate in these tests is accurate to about $\pm 10\%$.

Fig. 3 shows the variation of yield stress with strain rate in PET at room temperature. In this figure, results from the high-speed testing machine are combined with Instron test results. It can be seen that there is a smooth transition between the two test methods. The effective upper strain-rate limit is determined by the resonant frequency of the load cell and upper clamp system, which is about 7 kHz. To record the load accurately at least ten cycles at 7 kHz must elapse, giving a maximum strain rate of approximately 50 $sec^{-1}$. Fig. 2a shows a test at 51 $sec^{-1}$ where ripple is noticeable. The restriction imposed by the requirement that about ten elastic waves must traverse the sample and clamps would suggest a much higher limiting strain rate of $10^3$ $sec^{-1}$.

### 2.4. Measurement of stress, strain and strain-rate

The yield stress and strain were determined from the load and extension at the first maximum in load. Stresses were calculated from the reduced cross-sectional area, assuming that the samples deform at constant volume.

In the Instron tests, the extension was determined from the time given by the chart and the cross-head speed. In the high speed tests, when there was no observed slack, the extension was determined from the 0.5 cm marker pip trace. As described above, when slack was observed the extension was determined from the marker pips for no load.

The effective gauge length of the dumb-bell sample for calculating the maximum strain and strain rate from the clamp movement was calculated to be 3.70 cm, on the basis of linear behaviour. The effect of the tapering section was smaller as the behaviour became more non-linear, and the gauge length then tended towards the length of the narrow section.

The strains were always assumed to be small, strain and strain rate being calculated from the ratio of grip displacement or displacement rate to gauge length. Any corrections for finite strain would be small compared with the estimated 10% accuracy of the strain measurements.

### 2.5. Temperature measurement and control

The tensile tests were performed over the temperature range from $+60$ to $-190°$ C. In all cases the test temperature was measured by two copper–constantan thermocouples, one at each end of the sample.

Two systems were used to obtain the low and high temperatures. In the first, a small lagged copper jacket enclosed the sample while either cold nitrogen evaporated from liquid nitrogen in a Dewar vessel or hot air from a heated coil was blown through the jacket walls. This system was used for all the tests on the high-speed tester where there was limited space, and for temperatures below $-60°$ C in the Instron tests. Temperatures could be controlled to $\pm 2°$ C but only for a short period ($\sim 5$ min).

For Instron tests in the range $-60$ to $+60°$ C an environmental cabinet was used, which allowed temperature control of $\pm 1°$ C.

## 3. Results and discussion

### 3.1. General features

Load–elongation curves were determined over the temperature range $-196$ to $+50°$ C at strain rates of $4.5 \times 10^{-6}$, $4.5 \times 10^{-5}$, $4.5 \times 10^{-4}$, $4.5 \times 10^{-3}$, $4.5 \times 10^{-2}$, 0.98, 10.2 and 51 $sec^{-1}$. Strain rates below $10^{-1}$ $sec^{-1}$ were achieved with the Instron tensile testing machine and higher strain rates with the high-speed tensile testing machine.

In a previous publication [10], it was noted that essentially five different types of failure can be observed in amorphous PET over the range of temperatures from $-196°$ C to above the glass transition temperature $T_g$. These were termed brittle, ductile, necking rupture, cold drawing and uniform extension in order of increasing temperature of observation. Four of these five failure modes (excluding the ductile mode) have been discussed in some detail in a review article by Vincent [11]. These modes of failure are shown schematically in Fig. 4 which represents load–extension curves at a fixed strain rate for various temperatures. At high temperatures and low strain-rates but below $T_g$ the polymer yields in a well-defined deformation band and then cold draws. With decreasing temperatures or higher strain rates, a region of necking rupture is observed in which fracture occurs within a deformation band. At lower temperatures or higher strain rates plastic deformation leading to a load drop occurs but does not stabilize into a band. This is termed ductile fracture. At still higher strain-rates or lower temperatures brittle failure is obtained. A deformation map is given in Fig. 5 which indicates the nature of failure as a function of strain rate and temperature.

A number of features are clearly distinguishable

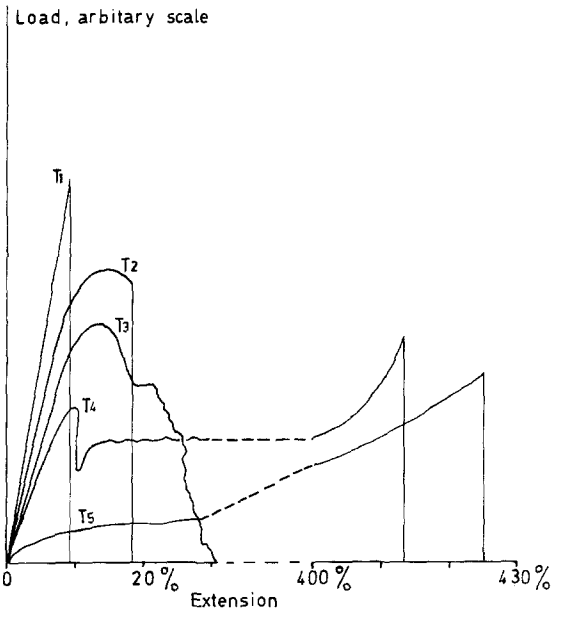


*Figure 4* Schematic load–extension curves at different temperatures showing the types of failure observed. Temperatures $T_1 < T_2 < T_3 < T_4 < T_g < T_5$ (K) $T_1$, brittle; $T_2$, ductile; $T_3$, necking rupture; $T_4$, cold drawing; $T_g$, glass transition temperature; $T_5$, uniform extension.

from consideration of these results which are to be presented in detail later. First, the brittle failure shows considerable scatter in the value of the failure stress and is almost temperature and strain-rate independent. Second, the yield behaviour is typified by a reproducible yield stress which is both strain-rate and temperature dependent. These features had already been noted over a much smaller range of strain rates in the previous publication [10]. One implication is that the brittle–ductile transition moves steadily to higher temperatures with increasing strain–rate as

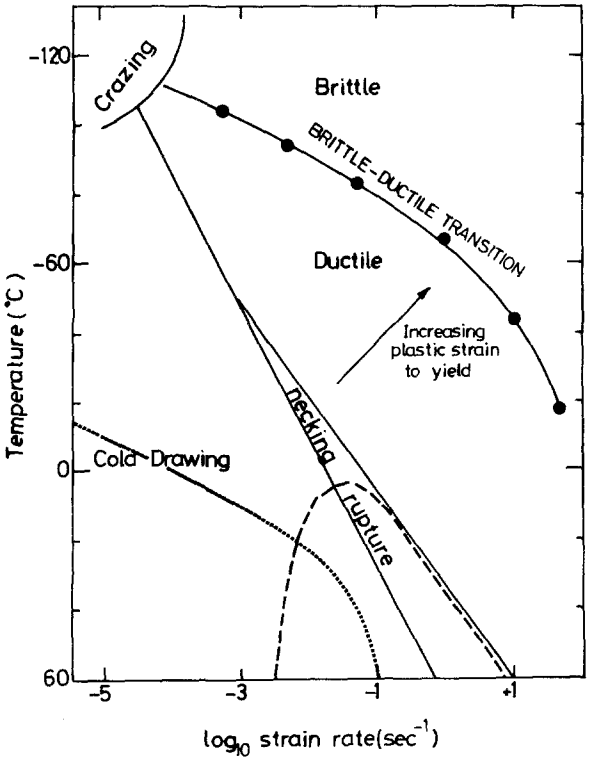


*Figure 5* Deformation map for amorphous PET.

TABLE I The yield stress value for different loading programmes at 22° C (see text)

| Loading programme | Yield stress (MPa) |
|---|---|
| 1 | 57 ± 1 |
| 2 | 62 ± 1 |
| 3 | 62 ± 1 |
| 4 | 61 ± 1 |

shown in Fig. 5. A further implication is that there is some merit in considering the yield and brittle failure regions separately in the first instance and this is the approach adopted in this paper. The fracture behaviour was considered in detail in a separate publication [12] with regard to the effects of crystallinity and molecular weight.

## 3.2. The yield behaviour

### *3.2.1. General considerations*

In this work the yield stress was calculated as the load at the first maximum on the load–extension curve, divided by the reduced cross-sectional area, calculated from the strain at this point assuming deformation at constant volume. The significance of this definition of the yield point lies in the fact that when the load is stationary, the elastic strains in the material and in the tensile testing machines are constant. Thus at the yield stress, the plastic strain rate produced in the sample by the stress is exactly equal to the imposed strain rate.

In general, the yield stress, $\sigma_y$, of a polymer is a function of both temperature and the entire strain history up to and including the yield point. Thus a complete theory of the yield behaviour would have to embrace the non-linear viscoelastic aspects and include the effects of interrupted loading programmes, etc. A subsidiary experiment, now to be described, provides some justification for ignoring such complexities in the first instance and assuming that the yield stress as measured in these experiments is a function only of strain rate and temperature.

Table I shows results for the yield stress determined for four different loading programmes. Programmes 1 and 2 were constant strain-rate tests at $4.5 \times 10^{-3}$ and $4.5 \times 10^{-2}\,\text{sec}^{-1}$, respectively. In programmes 3 and 4 a strain rate of $4.5 \times 10^{-3}\,\text{sec}^{-1}$ was applied up to approximately 90 and 98%, respectively, of the yield load at this strain rate, followed by a strain rate of $4.5 \times 10^{-2}\,\text{sec}^{-1}$. The results in Table I are averages for three samples in each case. There is some evidence in programme 4 that when some of the deformation occurs at a different strain-rate, the yield stress is not a unique function of the strain-rate at yield. The close agreement of programmes 3 and 4, however, suggests that these effects are second-order, and it will be reasonable to assume that for a constant strain-rate test yield stress is a function of strain rate only.

Fig. 6 shows the variation of strain at yield as a function of the yield stress at a strain rate of $4.5 \times 10^{-3}\,\text{sec}^{-1}$. Each point represents a different test temperature, but similar results would be obtained by changing the strain-rate and maintaining a constant temperature of test, as indicated in the figure. Also shown in Fig. 6 is the calculated linear-elastic

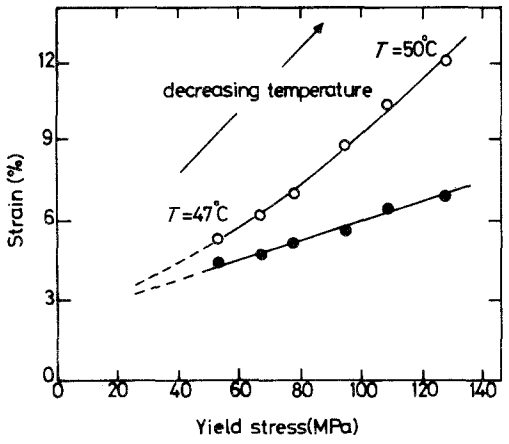


*Figure 6* Variation of yield strain (○) and elastic strain to yield (●) (yield stress/initial modulus) with yield stress ($\dot{\epsilon} = 4.5 \times 10^{-3}\,\mathrm{sec}^{-1}$).

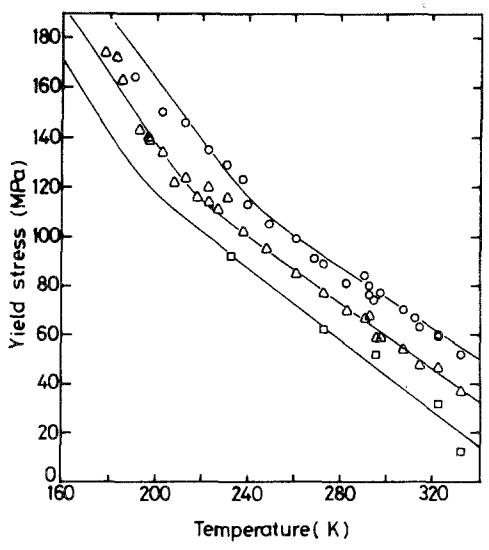


*Figure 7* Temperature dependence of the yield stress. Curves calculated from Equation 5 with best fit parameters listed in Table II. Strain rate ($\mathrm{sec}^{-1}$): (○) $4.68 \times 10^{-2}$), (△) $4.68 \times 10^{-4}$, (□) $4.68 \times 10^{-6}$.

contribution to the strain, using appropriate values of the modulus obtained from the initial slopes of the load–extension curves. It can be seen clearly from the figure that the strain at yield increases more rapidly with decreasing temperature or increasing strain-rate than the linear elastic contribution to the strain. This particular aspect of the yield behaviour is by-passed in our further discussions, where we will consider the strain-rate and temperature dependence in the light of the multiple Eyring process approach.

### 3.2.2. Detailed analysis of yield behaviour

Fig. 7 shows the yield stress as a function of temperature over four decades of strain rate. At higher temperatures, the yield stress showed a relatively constant temperature dependence which increased to a higher temperature dependence at lower temperatures. At a strain rate of $4.68 \times 10^{-2}\,\mathrm{sec}^{-1}$, the transition occurred at a temperature of $\sim 250$ K but the position of the transition shifted to lower temperatures at lower strain rates. At a strain rate of $4.68 \times 10^{-5}\,\mathrm{sec}^{-1}$, the transition occurred at $\sim 210$ K. Fig. 8 shows the strain-rate dependence of the yield at different temperatures. At low strain rates and high temperatures, a relatively low strain-rate dependence of the yield stress was observed but this

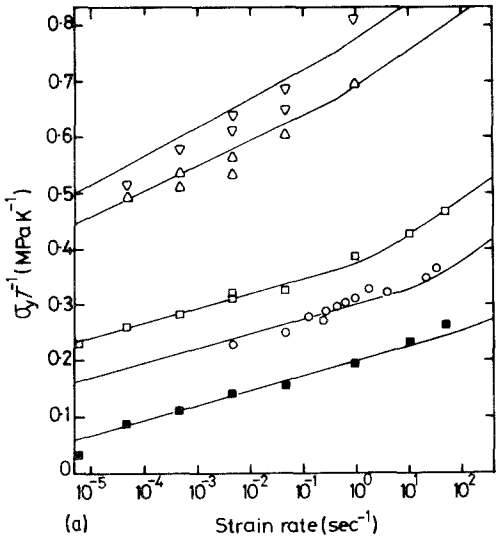


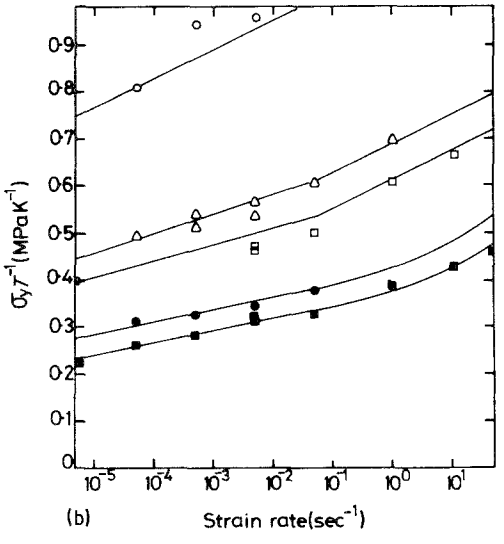


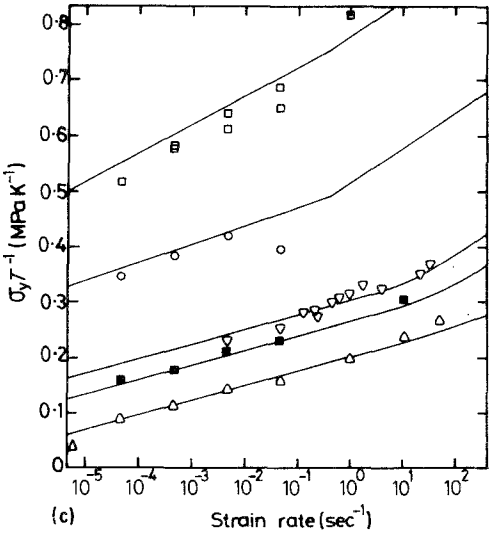


*Figure 8* Strain-rate dependence of the yield stress/temperature. Curves calculated from Equation 4 with best fit parameters listed in Table II. (a) Temperatures (K): (▽) 213, (△) 223, (□) 273, (○) 295, (■) 333. (b) Temperatures (K): (○) 183, (△) 223, (□) 233, (●) 261, (■) 273. (c) Temperatures (K): (□) 213, (○) 248, (▽) 295, (■) 308, (△) 333.

TABLE II Best fit parameters for Equation 4

| | Process 1 | Process 2 |
|---|---|---|
| $v$ ($nm^3$) | 1.21 | 0.86 |
| $\Delta H$ (kcal $mol^{-1}$) | 45 | 17.1 |
| $\ln \dot{\varepsilon}_0$ ($sec^{-1}$) | 50.9 | 32.9 |

changed to a high rate dependence at high strain rates and low temperatures.

This type of behaviour of the yield stress suggests that it can be fitted to two Eyring processes operating in parallel. All of the yield data obtained for the amorphous PET involving 171 yield points was fitted by computer, using least squares fitting techniques outlined in the previous paper [1], to Equation 4. Table II lists the six Eyring parameters obtained. The lines drawn in Figs 7 and 8a to c are calculated from these parameters and it can be seen that the overall fit is good.

For the case of polyethylene, the transitions in the strain-rate behaviour could be related to the mechanical relaxations observed in the linear viscoelastic behaviour of the material. Thompson and Woods [13] reported that the $\beta$ dynamic loss peak in amorphous PET occurred at 253 K at a frequency of 1.2 Hz. 1.2 Hz is approximately equivalent to a strain rate of $2 \times 10^{-1} sec^{-1}$. It has already been noted that the transition in the yield behaviour of PET occurred at 250 K at a strain rate of $4.68 \times 10^{-2} sec^{-1}$. Thus the change in slope seen in the yield behaviour in Fig. 7 is related to the onset of the $\beta$-relaxation. Moreover, Thompson and Woods [13] gave the activation energy of the $\beta$-relaxation as 17 kcal $mol^{-1}$, which is in remarkably good agreement with the value of 17.1 kcal $mol^{-1}$ found for process 2 in this material. It is, however, difficult to ascribe any molecular mechanism to the $\beta$-relaxation.

Fig. 7 suggests that in the high-temperature range only process 1 is effective. The value of 45 kcal $mol^{-1}$ for the activation energy of this process is consistent with previous values obtained for isotropic PET sheet by Duckett [14] and for amorphous undrawn PET fibre by Allison and Ward [15]. Inspection of Fig. 7 reveals the extreme strain-rate dependence of the yield stress in the vicinity of the conventional glass transition. Note, however, that Illers and Breuer [16] quote the activation energy for the dynamical mechanical $\alpha$-relaxation as $\sim 180$ kcal $mol^{-1}$, in sharp contrast with that measured from the yield stress here. Thus as was the case in our previous work on polyethylene [7], the nature of the high temperature, low strain rate yield process must remain obscure.

## References


1. Y. S. LAZURKIN, *J. Polym. Sci.* **30** (1958) 595.
2. R. E. ROBERTSON, *J. Appl. Polym. Sci.* **7** (1963) 443.
3. J. A. ROETLING, *Polymer* **6** (1965) 311.
4. C. BAUWENS-CROWET, J. A. BAUWENS and G. HOMES, *J. Polym. Sci. A2* **7** (1969) 735.
5. R. N. HAWARD and G. THACKRAY, *Proc. Roy. Soc. A* **302** (1968) 453.
6. G. HALSEY, H. J. WHITE and H. EYRING, *Test Res. J.* **15** (1945) 295.
7. R. W. TRUSS, P. L. CLARKE, R. A. DUCKETT and I. M. WARD, *J. Polym. Sci. Polym. Phys. Edn.* **22** (1984) 191.
8. J. S. FOOT, PhD thesis, Bristol University (1972).
9. L. E. AMORSKI and T. D. MECCA, *J. Appl. Polym. Sci.* **4** (1960) 332.
10. J. M. STEARNE and I. M. WARD, *J. Mater. Sci.* **4** (1969) 1088.
11. P. I. VINCENT, "Encylopedia of Polymer Science and Technology", Vol. 7 (Wiley, New York, 1967) p. 292.
12. J. S. FOOT and I. M. WARD, *J. Mater. Sci.* **7** (1972) 367.
13. A. B. THOMPSON and D. W. WOODS, *Trans. Faraday Soc.* **52** (1956) 1383.
14. R. A. DUCKETT, PhD thesis, Bristol University (1968).
15. S. W. ALLISON and I. M. WARD, *Brit. J. Appl. Phys.* **18** (1967) 1151.
16. K. H. ILLERS and H. BREUER, *J. Colloid Sci.* **18** (1963) 1.



*Received 2 June*
*and accepted 18 August 1986*